International Journal of
Nanoscience and Nanotechnology

Research Article 2025, Volume 21, Issue 1

Exploring Multiferroic Properties In New Lead-Free Ceramic $(Sr_{0.95}Ba_{0.05})(Mn_{0.5}Nb_{0.5})O_3$

Srikanta Behera[1], Raj Mohan Mohanty[2], Raj Kishore Mishra[3*], Sabyasachi Parida[4*], Muhammad Shahid Anwar[5], Priyabrata Nayak[6], B.S. Tripathy[7]

Received 10/24/2024
Accepted 2/8/2025

DOI:10.22034/ijnn.2025.2044142.2592

International Journal of Nanoscience and Nanotechnology

Abstract

A new lead-free ceramic material of complex perovskite structure (ABO3) with the formula (Sr0.95Ba0.05)(Mn0.5Nb0.5)O_3 has been prepared using a solid-state reaction technique. The X-ray diffraction pattern of $(Sr_{0.95}Ba_{0.05})(Mn_{0.5}Nb_{0.5})O_3$ at ambient temperature shows that the sample has a single-phase tetragonal perovskite structure. The surface morphology studied by scanning electron microscopy (SEM) shows the polycrystalline nature of the prepared material with grains of uniform size having few voids. The dielectric parameters (relative permittivity or dielectric constant and loss tangent) of the samples were determined over a wide range of frequency (100 Hz to 5MHz) and a temperature range of 25 ˚C to 250 ˚C. The overall frequency response of the material within this observed frequency window shows low-frequency relaxation phenomena and deviation from Debye-type behavior. At all frequencies, the permittivity shows a broad diffused peak at around 215 ˚C, which may be attributed to ferroelectric to paraelectric transition. The AC conductivity spectra obey Jonscher's universal power law. The optical band gap calculated from diffuse reflectance spectroscopy (DRS) data is 3.06 eV. Magnetization (M) in both zero-field-cooled (ZFC) and field-cooled (FC) modes measured at 0.05 T shows a gradual increase of magnetic field with a decrease in temperature below 300 K with a magnetic order transition below 40K. Also, the M-H curve at 10 K shows a nonlinear pattern with a small opening in the hysteresis loop, indicating some ferromagnetic component at low temperatures.

Keywords: Ferroelectric, Multiferroic, Ceramics, Impedance, Magnetic Order

How to cite this article

Behera S, Mohanty RM, Mishra RK, Parida S, Anwar MS, Nayak P, Tripathy BS. Exploring Multiferroic Properties In New Lead-Free Ceramic $(Sr_{0.95}Ba_{0.05})(Mn_{0.5}Nb_{0.5})O_3$. Int. J. Nanosci. Nanotechnol., 2025;1: 11-19. DOI: 10.22034/ijnn.2025.2044142.2592

1. Introduction

Because of the intrinsic capability of the perovskite structure to host ions of different sizes, a large number of dopants can be accommodated in the crystalline lattice [1-5]. Oxides with the perovskite structure, ABO_3, have a broad range of applications due to their remarkable properties, such as high dielectric constant, piezoelectric, ferroelectric, ferromagnetic, ferrimagnetic, and multiferroic properties, etc. [6-19]. Accommodating different cations at both the A-site and B-site of this structure, complex perovskites $(A_1\ A_2\ A_{3...})(B_1\ B_2\ B_3\ ...)O_3$ can be formed, which gives a wide scope to tailor the material properties by a suitable choice of cations. When complex perovskites contain two cations at the B-site that vary in ionic size and oxidation states, they have interesting dielectric and ferroelectric properties. Also, most of these cations are in their highest oxidation state with filled core shells. The high dielectric constant in these perovskites may appear due to the ordering of B-site cations in the structure[20-25]. It has been established that when lead occupies the A-site, the material shows good ferroelectric and multiferroic properties like Pb (Zr, Ti)O_3[2], $Pb(Fe_{0.5}Nb_{0.5})O_3$ [19], $Pb(Fe_{0.5}Ta_{0.5})O_3$ [3], etc. However, due to the toxicity of lead, the scientific community has been trying to replace lead with eco-friendly cations. The Gr-II cations have proved to be the most suitable candidates for lead-free complex perovskites like (Ba, Sr)TiO_3 [4]. These are safe and sustainable alternatives that also enhance dielectric behavior. It has been established that when the B-site of these complex perovskites accommodates both d^0 cations and d^n cations, the material gives both dipolar and magnetic order, leading to multiferroic properties [7-14]. This has motivated us to determine the dielectric, electrical, and magnetic properties of complex lead-free

[1,2,4] *Department of Physics, C.V.Raman Global University, Bhubaneswar, Odisha, India*

[3] *Department of Physics, Maharishi College of Natural Law, Bhubaneswar, Odisha, India*

[5] *CSIR-Instituteof Minerals and MaterialsTechnology, Bhubaneswar, Odisha, India*

[6] *CSIR-Instituteof Minerals and Materials Technology, Bhubaneswar, Odisha, India & Academy of Scientific and Innovative Research(AcSIR), Ghaziabad, Uttar Pradesh, India*

[7] *Department of Physics, ITER, Siksha 'O' Anusandhan University, Bhubaneswar, Odisha, India*

E-mail: rkm.phy@gmail.com; sabyasachi.parida@cgu-odisha.ac.in

perovskite $(Sr_{0.95}Ba_{0.05})(Mn_{0.5}Nb_{9.5})O_3$, where the A-site is occupied by Gr-II cations Sr^{2+} and Ba^{2+}, and the B-site is occupied by d^0 cation (Nb^{+5}) and d^n cation (Mn^{3+}). This type of complex perovskite ceramics, where the B site accommodates Mn+3 and Nb+5, and the A site is completely lead-free, has never been reported.

2. Experimental

$(Sr_{0.95}Ba_{0.05})(Mn_{0.5}Nb_{0.5})O_3$ with a polycrystalline structure was synthesized using AR-grade precursors: $SrCO_3$, $BaCO_3$ (98%, Loba Chemicals, India), Mn_2O_3 (98 %, Alfa Aesar), and Nb_2O_5 (99%, Loba Chemicals, India). The reactive powders were mixed mechanically in an appropriate stoichiometric ratio. The above powders were mixed completely under dry conditions for 1 hour in an agate mortar, followed by a wet treatment (e.g., methanol) for 2 hours to achieve a homogeneous mixture. Then, the mixed powder in a platinum crucible was calcined at 1200 °C for 6 h. The powder so obtained after calcination was cold pressed into pellets (dia. 10 mm) under an uniaxial pressure of $5x10^6 N/m^2$ using polyvinyl alcohol (PVA) as the binder. The pellets were then sintered at 1250 °C for 6 h. The pellets were finally coated with silver paint, and then dried at 150 °C for 2 h prior to electrical measurements.

To determine the compound formation, x-ray diffraction (XRD) studies were carried out (X-ray powder diffractometer, Rigaku, PANalytical X'Pert). The XRD pattern of the calcined powder was recorded at room temperature with "CuK_α radiation (λ = 1.5405 Å). An X-ray study was carried out in a wide range of Bragg angles (20° ≤2θ ≤80°) at a scan speed of 3°/minute. Micro Raman spectroscopic behavior was studied via a Renishaw Invia Reflex (UK) spectrometer. Surface morphology has been studied by scanning electron microscopy (ZEISS-EVO 18). The elemental composition of the material was measured by EDAX (OCTANE ELECT). The sample pellets were gold sputtered prior to being scanned under a high-resolution electron beam of the SEM. Electrical analysis was carried out using a computer-controlled impedance analyzer (HIOKI LCR METER) in the frequency range from 100Hz to 5MHz and in a temperature range of 25 °C to 250 °C. The acquisition of data was monitored as a function of frequency and temperature. The optical property (diffuse reflectance spectroscopy (DRS)) was studied using the Thermo Scientific Evolution 220 model in the range of 190–1100 nm. The magnetic measurements were taken in SQUID-VSM.

3. Results and Discussion

3.1. Structure and microstructure

Figure 1(a) depicts the X-ray diffraction pattern of $(Sr_{0.95}Ba_{0.05})(Mn_{0.5}Nb_{0.5})O_3$ at ambient temperature. The acquired findings show that the sample has a tetragonal perovskite structure as a single phase without any additional impurity peaks. To substantiate this claim, the powder underwent Rietveld refinement. Fullprof software [26] was used to carry out the structural refinement. After refinement of the samples, the numbers obtained from R-values and χ^2 are recorded. It shows the tetragonal structure of space group I 4/m c m. The success of a Rietveld refinement is evaluated by the difference plot between observed and calculated patterns (Figure 1(b)). As shown in the figure, a good agreement between the calculated and experimental data was achieved, with a χ^2 value of 3.15 (R_p = 30.7, R_{wp} = 45.3, and R_{exp} = 20.09). The compound crystallizes in the tetragonal phase with refined lattice parameters a: 5.595601 Å, b: 5.595601 Å, c: 7.952655 Å, with c/a ratio of 1.421 and space group I 4/mcm. Table 1 provides the atomic site positions and occupancies of each element, as determined through refinement. The refined structure has been obtained using data given in Table 1 and the VESTA program (version 3.0 for Windows).

Figure 2 shows SEM images and EDAX of the sintered pellets of $(Sr_{0.95}Ba_{0.05})(Mn_{0.5}Nb_{0.5})O_3$. The micrograph shows uniform grains with few voids in the prepared sample. The EDAX confirms the formation of the sample using a proper stoichiometric ratio.

3.2. Spectroscopy

Figure 3. shows room temperature micro-Raman data for all the samples of $(Sr_{0.95}Ba_{0.05})(Mn_{0.5}Nb_{0.5})O_3$. The peak at 577 cm^{-1} may be assigned to B-O displacement, while the peak at 694 cm^{-1} may be due to the symmetric stretching

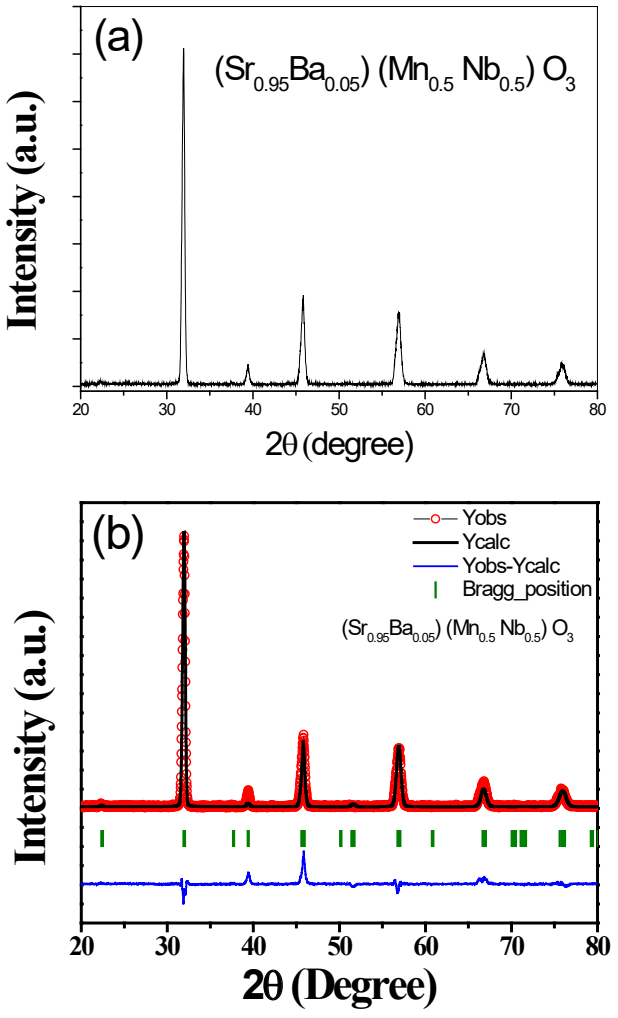

Figure 1. (a) Room temperature XRD and (b) Rietveld refinement of $(Sr_{0.95}Ba_{0.05})(Mn_{0.5}Nb_{0.5})O_3$

Table 1. The atomic site position and occupancy of each element obtained through refinement fitting of $(Sr_{095}Ba_{0.05})(Mn_{0.5}Nb_{0.5})O_3$

Atoms	X	Y	Z	Occupancy
Sr	0.00000	0.50000	0.25000	0.95000
Ba	0.00000	0.50000	0.25000	0.05000
Mn	0.00000	0.00000	0.00000	0.50000
Nb	0.00000	0.00000	0.00000	0.50000
O1	0.00000	0.00000	0.25000	1.00000
O2	0.25000	0.50000	0.00000	1.00000

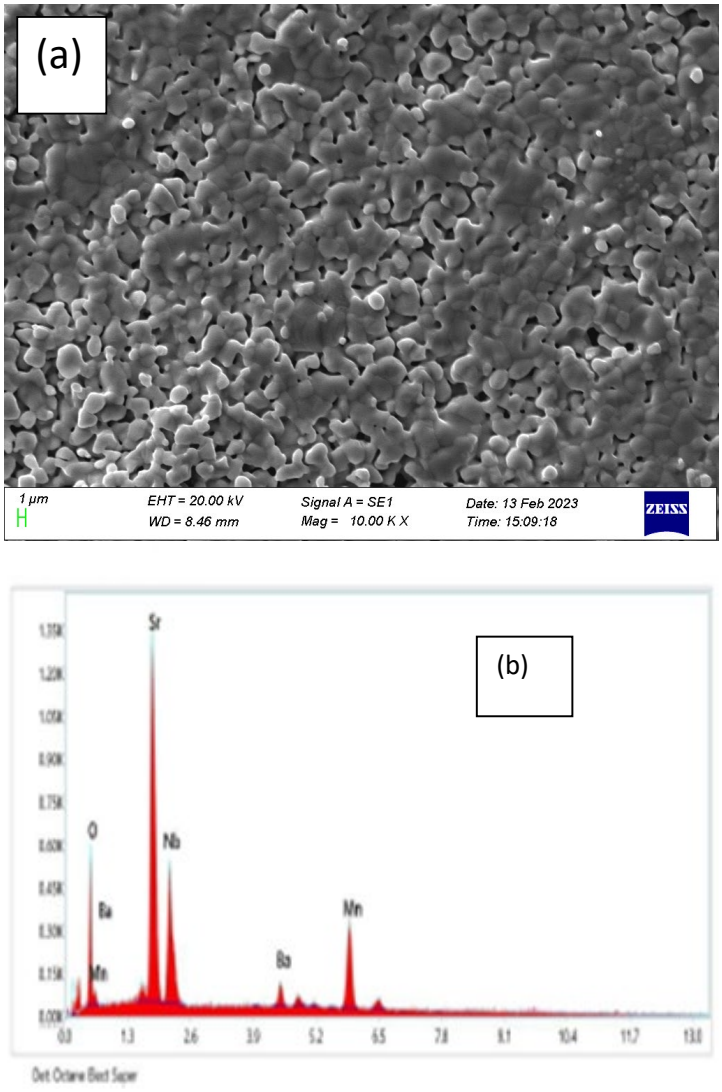

Figure 2. (a) SEM image, (b) EDAX of the sintered $(Sr_{0.95}Ba_{0.05})(Mn_{0.5}Nb_{0.5})O_3$

of BO_6 octahedra. The broadening of peaks may be due to lattice disorder [3].

3.3. Dielectric and electrical properties

Figure 4. shows the Tauc plot drawn from the DRS data of the sample obtained at room temperature. The optical band gap calculated is 3.06 eV. This high value of band gap is typical of ferroelectric oxides. The charge transfer between Nb-O ions and the electronic transitions of Mn $^{+3}$ ions, along with a high state of disorder, may be responsible for this band gap value in the material [27,28].

Figure 5. shows the frequency response of dielectric properties, i.e., the variation of relative permittivity and tan δ (inset) with the frequency of $(Sr_{0.95}Ba_{0.05})(Mn_{0.5}Nb_{0.5})O_3$ at different temperatures. It shows a marked dispersive characteristic in both the permittivity and loss tangent pattern. A very high value of permittivity, as well as loss, shows that the material is lossy. This lossy behavior of the sample may be expected because of the oxygen ion vacancies produced by the varying oxidation states of Mn. Both ε_r and tan δ values decrease with increasing frequency, which is a typical behaviour of dielectric and

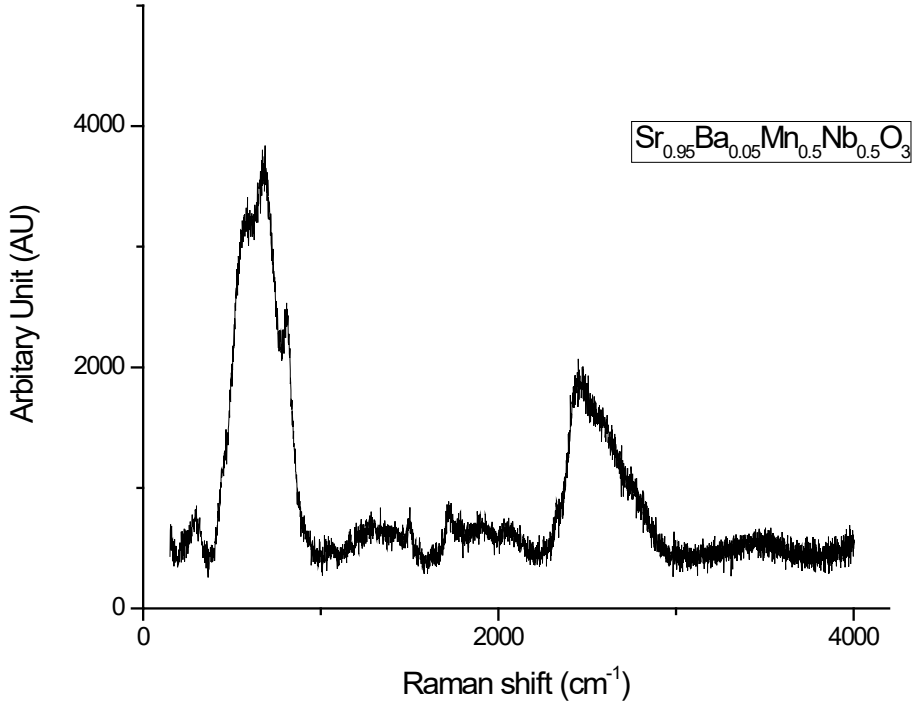

Figure 3. Room temperature Micro Raman spectra of all $(Sr_{0.95}Ba_{0.05})(Mn_{0.5}Nb_{0.5})O_3$ samples.

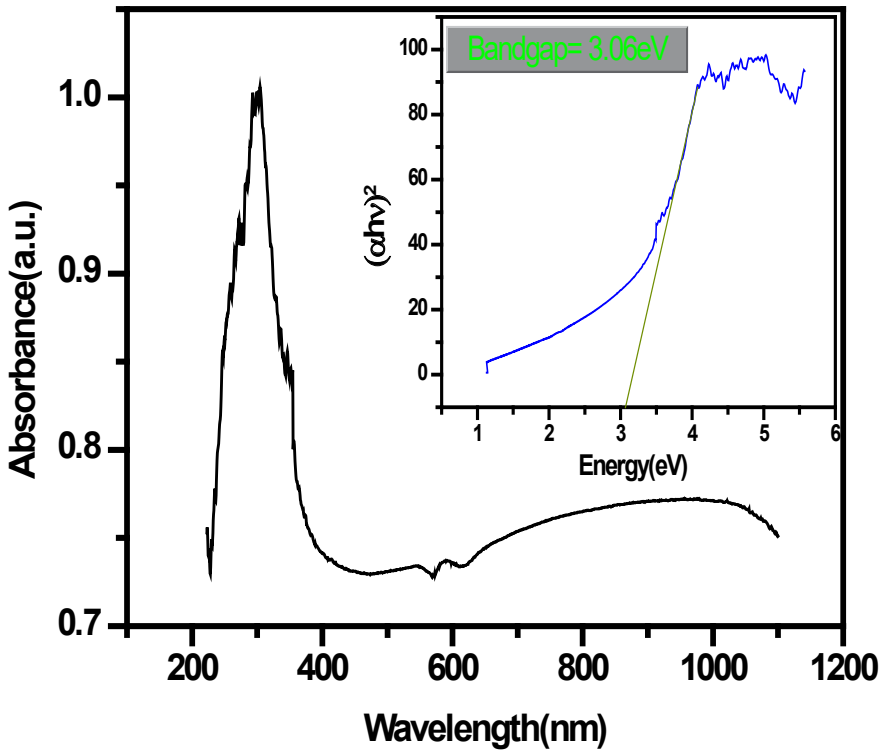

Figure 4. Tauc plot of room temperature DRS data of $(Sr_{0.95}Ba_{0.05})(Mn_{0.5}Nb_{0.5})O_3$

ferroelectric materials. It is known that permittivity, which is a measure of total polarization, has different components like ionic, electronic, dipolar, and space charge or interfacial, which arise at different stages of a material response to varying temperature and frequency of the applied alternating field, each of which involves a short-range displacement of charges. With increasing frequency, some of the dynamic polarization phenomena cease [20-25]. The overall frequency response of the material within this observed frequency window may be attributed to low-frequency relaxation phenomena, deviation from Debye-type behavior, and possible grain boundary barrier effect [29]. To gain more insight into the electrical microstructure, more rigorous studies such as

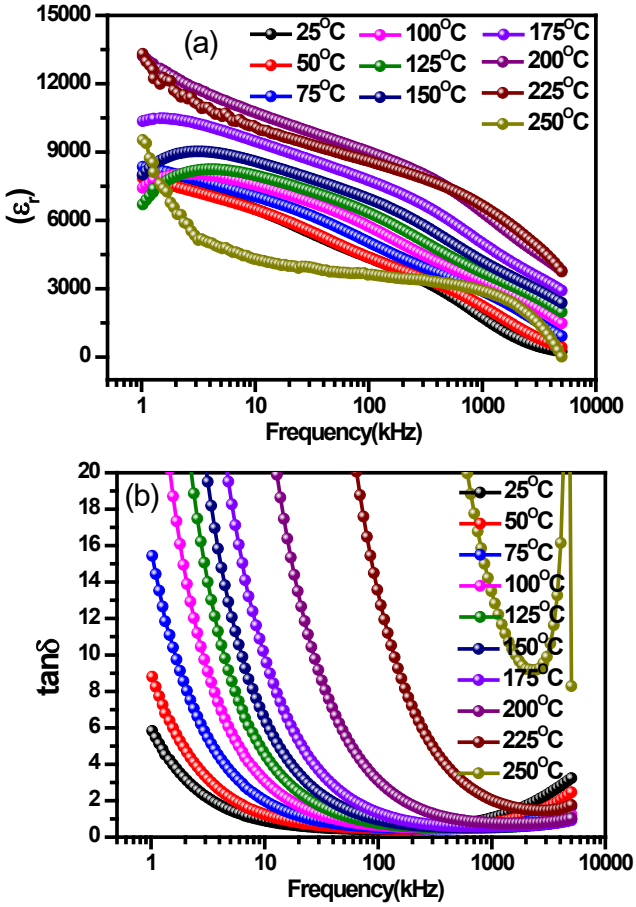

Figure 5. The variation of (a) relative permittivity (ε_r) and (b) dielectric loss (inset) with frequency of $(Sr_{0.95}Ba_{0.05})(Mn_{0.5}Nb_{0.5})O_3$ at different temperatures

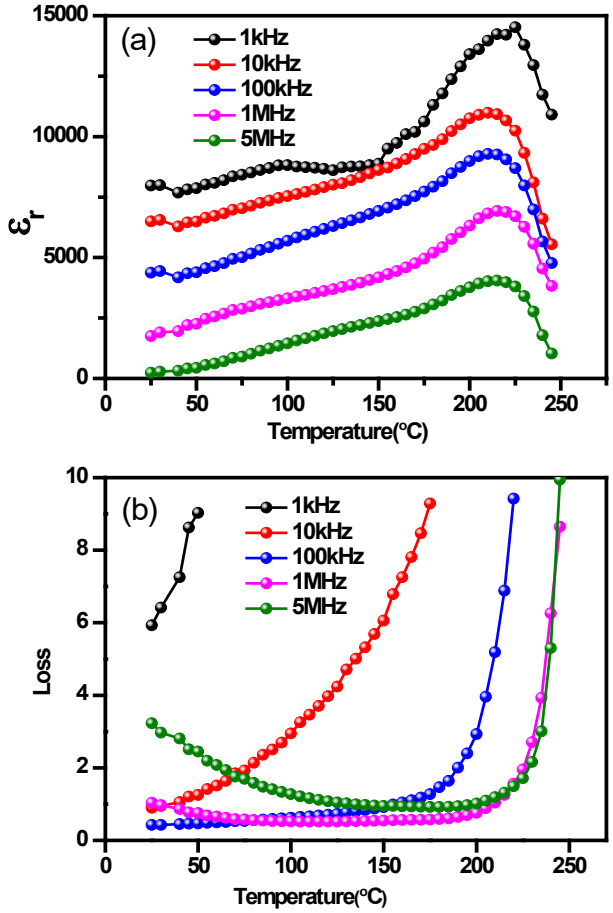

Figure 6. Variation of relative permittivity (a) and dielectric loss (b) with temperature of $(Sr_{0.95}Ba_{0.05})(Mn_{0.5}Nb_{0.5})O_3$ at different frequencies.

impedance spectroscopy in a wide frequency window are required.

Figure 6 (a) and (b) show the variation of the relative permittivity (εr) and the loss tangent tan δ with the temperature at different frequencies, i.e., 10 kHz, 100 kHz, and 1 MHz and 5 MHz, respectively. Both ε_r and tan δ for the material show very high values. They increase with temperature for all frequencies. The value of permittivity gradually increases with temperature, and at all frequencies, the permittivity shows a broad diffused peak around 215 °C while the value of loss increases to an extremely high value with increasing temperature. The exceptionally high value of relative permittivity with high tan δ shows the lossy behavior of the material with long-range conductive species. The diffused peak in permittivity at 215 °C may be attributed to ferroelectric to paraelectric transition. The lossy behavior may be attributed to oxygen ion vacancies due to the fluctuation of oxidation states of Mn within the oxygen octahedra.

Figure 7 shows the variation of real (Z') and imaginary parts of impedance (Z") as a function of frequency at different temperatures. The variation of real (Z') impedance as a function of frequency shows a low-frequency dispersive region followed by a merger into a plateau region. Also, the value of Z' decreases both with increasing temperature and frequency. The decrease of Z' with the rise of temperature is a typical semiconducting property with the negative temperature coefficient of resistance (i.e., NTCR type behavior), while the decrease of Z' with increasing frequency and finally merging on a plateau irrespective of temperature shows a thermally activated AC conductivity and release of space charge. These results indicate a possibility increase in the AC conductivity of the material with a rise in temperature in the high-frequency region, possibly due to the release of space charge as a result of a lowering of the barrier properties of the material.

The loss spectrum (variation of imaginary impedance (Z") with frequency) at different temperatures in Figure 7 shows the appearance of peaks at a characteristic frequency, dependent on temperature and can be related to the type and strength of the electrical relaxation phenomenon occurring in the material. A significant broadening of the peaks with the rise in temperature, and their asymmetric nature suggest the presence of a temperature-dependent relaxation process with the spread of relaxation time [19]. The magnitude of Z" peaks decreases while the width of the peaks increases with increasing temperature.

The scaling behaviour of the loss spectrum (variation of imaginary impedance (Z") with frequency) is displayed in the master curve (Figure 8), which shows all the curves

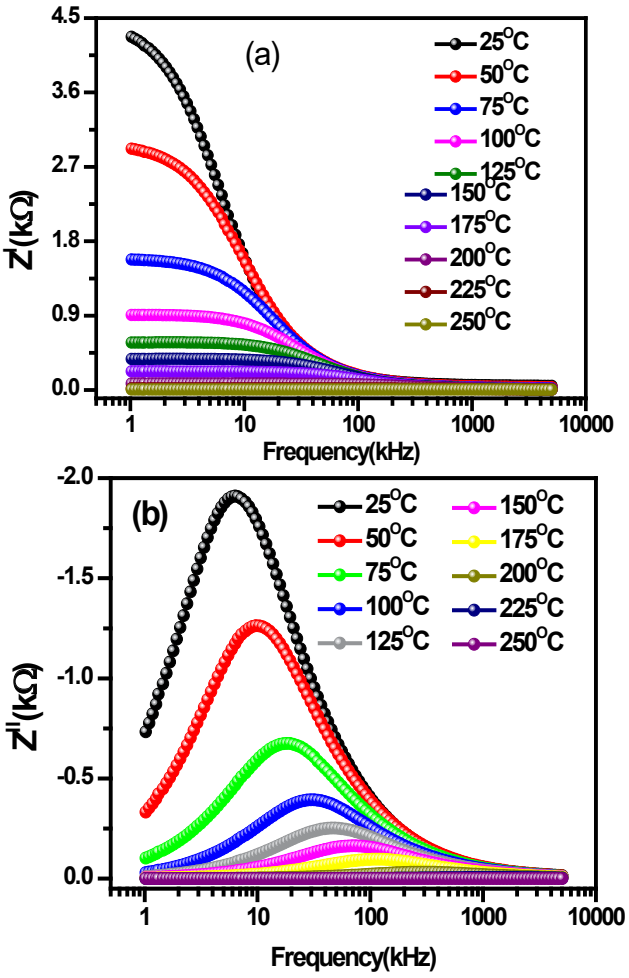

Figure 7. Variation of real (Z') and imaginary (Z") parts of impedance of $(Sr_{0.95}Ba_{0.05})(Mn_{0.5}Nb_{0.5})O_3$ with frequency at different temperatures.

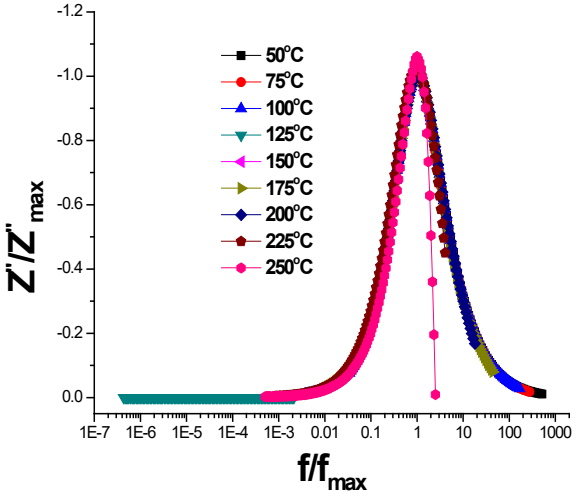

Figure 8. Plot of imaginary (Z") part of impedance with Z"max

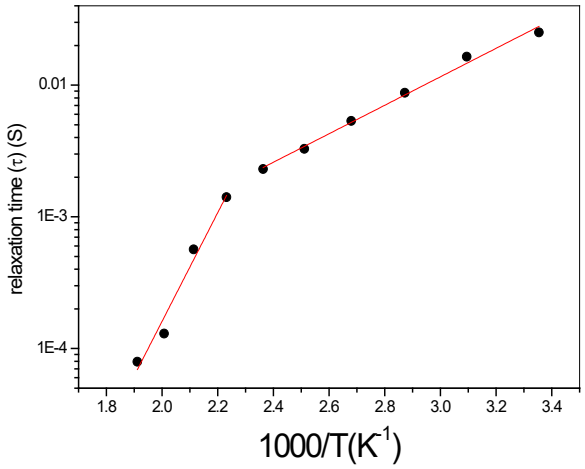

Figure 9. Variation of relaxation time for impedance with inverse temperature of $(Sr_{0.95}Ba_{0.05})(Mn_{0.5}Nb_{0.5})O_3$

are merging into a single one. This shows that the relaxing species are independent of temperature.

From the peaks of the loss spectrum, the relaxation time is calculated from the frequency at which the peak was observed. At the peak, the most probable relaxation is defined by the condition $\omega \tau = 1$. It is found that the relaxation time obeys the Arrhenius relationship: $\tau = \tau_o \exp(-E_a / kBT)$, where τ_o is the pre-exponential factor, and E_a is the activation energy. Figure 9 shows a plot of log τ *vs*. 1000/*T*. The value of E_a is estimated using the linear least squares that fit the data points. The graph clearly indicates two different linear regions at lower and higher temperature ranges, respectively. The two regions have two different activation energies, indicating different relaxation phenomena occurring at the lower and higher temperature ranges.

The activation energy calculated in the low-temperature range is 0.21 eV, and that in the high-temperature range is 0.81 eV. This marked difference in the activation energy is due to the role of oxygen ion vacancies at higher temperatures.

The conductivity spectra (i.e. the variation of a.c. conductivity (σ_{ac}) as a function of frequency) at different temperatures (25– 225 ˚C) are shown in Figure 10. At almost all temperatures, the spectra show a low-frequency plateau region followed by a high-frequency dispersion. The frequency-independent plateau in the low-frequency range is associated with the DC conductivity, σ_{dc}. This plateau region extends toward higher frequencies with increasing temperature. This type of conductivity behavior is well explained by Jonscher's power law [30] given by $\sigma(\omega) = \sigma_{dc} + A\omega^n$, where n is the frequency exponent ($0 \leq n \leq 1$), and A is a pre-exponential factor.

The material shows NTCR behavior like that of a semiconductor. The overall dielectric response, along with the heterogeneous conduction process, indicates that the material might have a diffused ferroelectric transition near 215 ˚C along with oxygen ion vacancies (V_O) induced dielectric relaxation, conductivity contribution to the dielectric matrix, and space charge polarization [31-33].

3.4. Magnetic properties

Figure 11(a) shows the magnetization (M) in both zero-field-cooled (ZFC) and field-cooled (FC) modes measured at 0.05 T of the $(Sr_{0.95}Ba_{0.05})(Mn_{0.5}Nb_{0.5})O_3$ ceramic sample. Magnetization increases gradually with the decrease

in temperature below 300 K, and around 40 K, and a small kink is observed at both magnetic fields without any observable shift in temperature. Further, there is no bifurcation in ZFC and FC magnetization modes around this kink, indicating a thermodynamic transition. However, a tendency of bifurcation between ZFC and FC starts at 10 K. The kink at 40 K indicates a magnetic ordering transition. The magnetization again increases continuously below this kink temperature, showing the existence of weak ferromagnetism. The effect of weak ferromagnetism at low temperatures is evident from the nonlinearity in the M–H hysteresis loop with a small opening in the loop at 10 K, as shown in Figure 11(b). It has been established that the magnetic order in perovskites can show both antiferromagnetic and ferromagnetic components. This type of metastable magnetic state in the polycrystalline material is observed in systems where ferromagnetic interactions are introduced randomly in a predominantly antiferromagnetic matrix. Here, Mn^{3+} is in a high-spin state, but the distribution of Nb^{5+} and Mn^{3+} are random at the B-site. Therefore, some of the super exchange interactions may give rise to the observed weak ferromagnetism and a random distribution of ferromagnetic interactions in the present system. Thus, it may be concluded that the distribution of Nb^{5+} and Mn^{3+} is actually random in our sample, which also has a significant effect on its dielectric properties. Nevertheless, this noteworthy low-temperature feature needs to be investigated in detail to ascertain its nature and origin, as well as its relation to the magnetoelectric coupling in this system. From a geometry point of view, the antiferromagnetism is based on 180° of the B-O-B' bond angle, and the bending of the B-O-B' bonding in distorted perovskites would give rise to additional magnetic interaction. By decreasing the exchange interaction and increasing the Dzyaloshinskii-Moriya interaction, weak ferromagnetic order might be induced [3, 19, 34].

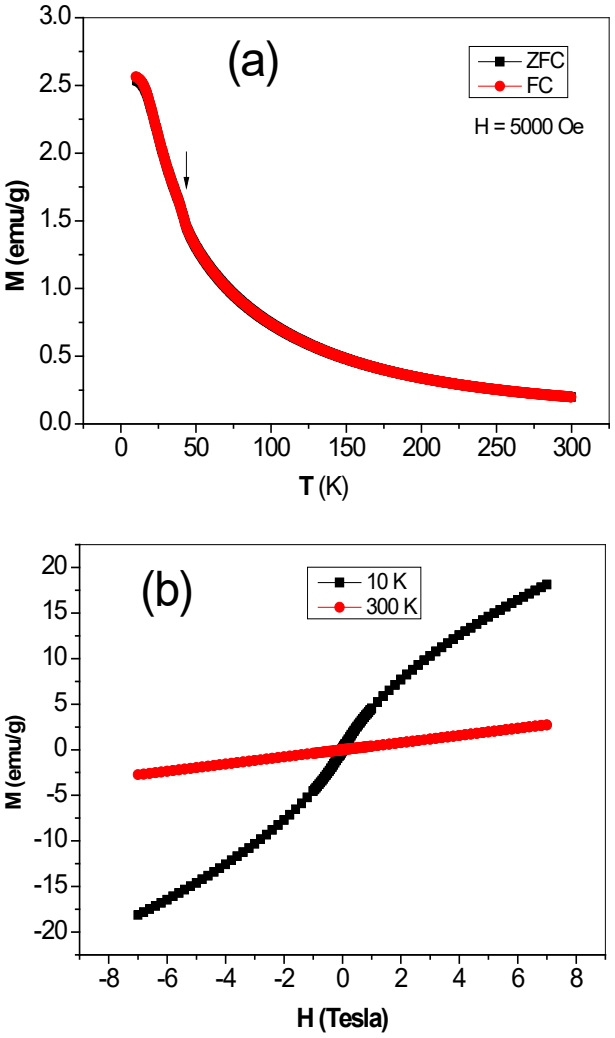

Figure 11. (a) Magnetization (M) vs. (T) graph in ZFC and FC mode at 0.05 T and Fig.11(b) Magnetization (M) vs. Field (H) at 10 K and 300 K of $(Sr_{0.95}Ba_{0.05})(Mn_{0.5}Nb_{0.5})O_3$

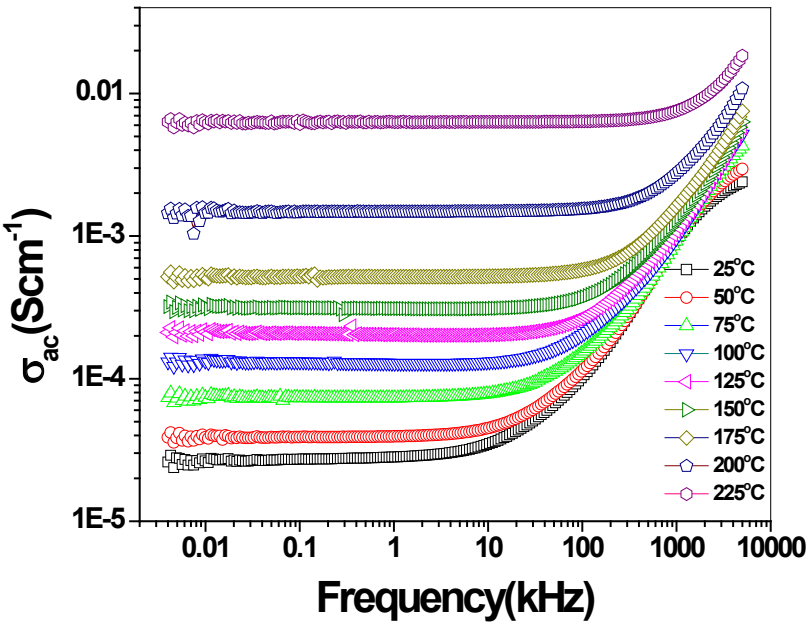

Figure 10. Variation of ac conductivity with frequency at different temperatures of $(Sr_{0.95}Ba_{0.05})(Mn_{0.05}Nb_{0.052})O_3$

Conclusion

The polycrystalline ceramic sample of $(Sr_{0.95}Ba_{0.05})(Mn_{0.5}Nb_{0.5})O_3$ was prepared using a solid-state technique. All the materials are formed in a single perovskite phase, which is confirmed by the room temperature XRD data. The structural analysis shows the formation of the materials in a single tetragonal structure. The frequency response of the dielectric properties of $(Sr_{0.95}Ba_{0.05})(Mn_{0.5}Nb_{0.5})O_3$ shows a strong low-frequency dispersion. The material shows a very high permittivity value along with high loss. The material shows a diffused phase transition at 215 ˚C in the temperature dependence of the permittivity at all measured frequencies. The impedance variation with temperature at different frequencies shows NTCR behavior and temperature-dependent relaxation phenomena. The ac conductivity obeys Jonscher's power law. The overall dielectric response, along with the heterogeneous conduction process, indicates that the material might have a diffused ferroelectric transition near 215 ˚C along with oxygen ion vacancies (V_O) induced dielectric relaxation, conductivity contribution on the dielectric matrix, and space charge polarization. The magnetization (M) vs. temperature (T) in both zero-field-cooled (ZFC) and field-cooled (FC) modes measured at 0.05 T, shows a magnetic order transition below 40 K. A small opening in the M-H hysteresis loop at 10 K shows weak ferromagnetism in the material.

Author Contributions

Conceptualization: Srikanta Behera, Raj Kishore Mishra, Sabyasachi Parida, Raj Mohan Mohanty; Methodology: Srikanta Behera, Raj Mohan Mohanty, Muhammad Shahid Anwar, Priyabrata Nayak, B.S.Tripathy; Formal analysis and investigation: Srikanta Behera, Raj Mohan Mohanty, Raj Kishore Mishra, Muhammad Shahid Anwar, Priyabrata Nayak, B.S.Tripathy; Writing - Original draft preparation: Srikanta Behera, Raj Kishore Mishra ; Writing - Review and Editing: Srikanta Behera, Raj Kishore Mishra, Sabyasachi Parida,; Supervision: Raj Kishore Mishra, Sabyasachi Parida.

Funding

No funding was received to conduct this study.

Ethical Statement

All authors have read and agreed to the final version of the manuscript. The work is original and it has not been communicated or published anywhere. The authors declare no conflict of interest.

References

1. Haertling GH. Ferroelectric ceramics: history and technology. J Am Ceram Soc. 1999;82(4):797-818. https://doi.org/10.1111/j.1151-2916.1999.tb01840.x
2. Kang MG, Jung WS, Kang CY, Yoon SJ. Recent progress on PZT based piezoelectric energy harvesting technologies. Actuators. 2016;5(5):1-17. https://doi.org/10.3390/act5010005
3. Sanchez DA, Ortega N, Kumar A, Roque-Malherbe R, Polanco R, Scott JF, et al. Symmetries and multiferroic properties of novel room-temperature magnetoelectrics: lead iron tantalate - lead zirconate titanate (PFT/PZT). AIP Adv. 2011;1:042169. https://doi.org/10.1063/1.3670361
4. Song Z, Liu H, Lanagan MT, Zhang S, Hao H, Cao M, et al. Thermal annealing effects on the energy storage properties of BST ceramics. J Am Ceram Soc. 2017;100(1):1-8. https://doi.org/10.1111/jace.14903
5. Elangovan NK, Kannadasan R, Beenarani BB, Alsharif MH, Kim MK, Inamul ZH. Recent developments in perovskite materials, fabrication techniques, band gap engineering, and the stability of perovskite solar cells. Energy Rep. 2024;11:1171-1190. https://doi.org/10.1016/j.egyr.2023.12.068
6. Yáñez-Vilar S, Mun ED, Zapf VS, Ueland BG, Gardner JS, Thompson JD, et al. Multiferroic behavior in the new double-perovskite Lu_2MnCoO_6. Phys Rev B. 2011;84:134427. https://doi.org/10.1103/PhysRevB.84.134427
7. Lu C, Wu M, Lin L, Liu JM. Single-phase multiferroics: new materials, phenomena, and physics. Natl Sci Rev. 2019;6(4):653-668. https://doi.org/10.1093/nsr/nwz091
8. Liu S, Xiang F, Cheng Y, Luo Y, Sun J. Multiferroic and magnetodielectric effects in multiferroic Pr_2FeAlO_6 double perovskite. Nanomaterials. 2022;12(17):3011. https://doi.org/10.3390/nano12173011
9. Liu H, Xue Y. A brief review on perovskite multiferroics. Ferroelectrics. 2017;507(1):69-85. https://doi.org/10.1080/00150193.2017.1283171
10. Weston L, Cui XY, Ringer SP, Stampfl C. Multiferroic crossover in perovskite oxides. Phys Rev B. 2016;93:165210. https://doi.org/10.1103/PhysRevB.93.165210
11. Acosta M, Novak N, Rojas V, Patel S, Vaish R, Koruza J, et al. $BaTiO_3$-based piezoelectrics: fundamentals, current status, and perspectives. Appl Phys Rev. 2017;4:041305. https://doi.org/10.1063/1.4990046
12. Hill NA. Why are there so few magnetic ferroelectrics? J Phys Chem B. 2000;104(29):6694-6709. https://doi.org/10.1021/jp000114x
13. Spaldin NA, Fiebig M. The renaissance of magnetoelectric multiferroics. Science. 2005;309(5733):391-392. https://doi.org/10.1126/science.1113357
14. Eerenstein W, Mathur ND, Scott JF. Multiferroic and magnetoelectric materials. Nature. 2006;442(7104):759-763. https://doi.org/10.1038/nature05023
15. Wu J, Mao S, Ye ZG, Zhaoxiong X, Lansun Z. Room-temperature ferromagnetic/ferroelectric $BiFeO_3$ synthesized by a self-catalyzed fast reaction process. J Mater Chem. 2010;20(31):6512-6516. https://doi.org/10.1039/c0jm00729c
16. Khelifi H, Zouaria I, Al-Hajry A, Abdelmoula N, Mezzane D, Khemakhem H. AC conductivity and ferroelectric phase transition of $Bi_{0.7}(Ba_{0.8}Sr_{0.2})_{0.3}Fe_{0.7}Ti_{0.3}O_3$ ceramic. Ceram Int. 2015;41(10 Pt B):12958-12966. https://doi.org/10.1016/j.ceramint.2015.06.139
17. Mishra RK, Pradhan DK, Choudhary RNP, Banerjee A. Effect of yttrium on improvement of dielectric properties and magnetic switching behavior in $BiFeO_3$. J Phys Condens Matter. 2008;20(4):045218. https://doi.org/10.1088/0953-8984/20/04/045218
18. Liu S, Xiang F, Cheng Y, Luo Y, Sun J. Multiferroic and magnetodielectric effects in multiferroic Pr_2FeAlO_6 double perovskite. Nanomaterials. 2022;12(17):3011. https://doi.org/10.3390/nano12173011
19. Mishra RK, Choudhary RNP, Banerjee A. Bulk permittivity, low frequency relaxation and the magnetic properties of $Pb(Fe_{1/2}Nb_{1/2})O_3$ ceramics. J Phys Condens Matter. 2010;22(2):025901. https://doi.org/10.1088/0953-8984/22/2/025901
20. Raevski IP, Prosandeev SA, Bogatin AS, Malitskaya MA, Jastrabik L. High dielectric permittivity in $A(Fe_{1/2}B_{1/2})O_3$ nonferroelectric perovskite ceramics (A = Ba, Sr, Ca; B = Nb, Ta, Sb). J Appl Phys. 2003;93(7):4130-4136. https://doi.org/10.1063/1.1558205

21. Krimech F, Sayouri S, Zouhairi M, El ghadraoui, Elbasset A. Structure and dielectric properties of sol-gel processed $Ba(Fe_{1/2}B_{1/2})O_3$ ceramics. Int J Curr Res. 2015;7(12):23584-23591.
22. Phatungthane T, Jaita P, Rujijanagul G. Structural, dielectric, and impedance study on ZnO doped $Sr(Fe_{0.5}Nb_{0.5})O_3$ ceramics. Phys B Condens Matter. 2019;556:103-107. https://doi.org/10.1016/j.physb.2018.12.023
23. Sinha TP. Dielectric relaxation in $SrFe_{1/2}Nb_{1/2}O_3$. J Appl Phys. 2006;99(1):014109. https://doi.org/10.1063/1.2160712
24. Sanjoom R, Jaita P, Chokethawai K, Randorn C, Watcharapasorn A, Phatungthane T, et al. Colossal dielectric constants in $Sr(Fe_{0.5}Nb_{0.5})_{1-x}Mn_xO_3$ prepared by a modified solid-state reaction technique. Ferroelectrics. 2022;601(1):9-23. https://doi.org/10.1080/00150193.2022.2130763
25. Kumar P, Sharma AK, Singh BP, Sinha TP, Singh NK. Dielectric relaxation in complex perovskite oxide $Sr(Gd_{0.5}Nb_{0.5})O_3$. Mater Sci Appl. 2012;3(5):369-376. https://doi.org/10.4236/msa.2012.36053
26. Rodríguez-Carvajal J. FullProf 2000, version July. Gif-sur-Yvette (France): Laboratoire Léon Brillouin, CEA/Saclay; 2001.
27. Pascual-Gonzalez C, Schileo G, Murakami S, Khesro A, Wang D, Reaney IM, et al. Continuously controllable optical band gap in orthorhombic ferroelectric $KNbO_3$-$BiFeO_3$ ceramics. Appl Phys Lett. 2017;110(17):172902. https://doi.org/10.1063/1.4982600
28. Wang F, Grinberg I, Rappe AM. Semiconducting ferroelectric photovoltaics through Zn^{2+} doping into $KNbO_3$ and polarization rotation. Phys Rev B. 2014;89:235105. https://doi.org/10.1103/PhysRevB.89.235105
29. Zhang N, Fang L. High dielectric constant and dielectric relaxations in $La_{2/3}Cu_3Ti_4O_{12}$ ceramics. Materials. 2022;15(13):4526. https://doi.org/10.3390/ma15134526
30. Jonscher AK. A new understanding of the dielectric relaxation of solids. J Mater Sci. 1981;16(8):2037-2060. https://doi.org/10.1007/BF00542364
31. Sanjoom R, Jaita P, Chokethawai K, Randorn C, Watcharapasorn A, Phatungthane T, et al. Colossal dielectric constants in $Sr(Fe_{0.5}Nb_{0.5})_{1-x}Mn_xO_3$ prepared by a modified solid-state reaction technique. Ferroelectrics. 2022;601(1):9-23. https://doi.org/10.1080/00150193.2022.2130763
32. Ansari MA, Jahan N. A novel co-precipitation route for the synthesis of pure and Ni-doped CuO nanoparticles: effect of doping on structural, optical, and electrical properties. Int J Nanosci Nanotechnol. 2023;19(2):65-76. https://doi.org/10.22034/ijnn.2023.555186.2219
33. Iyer NV, Agawane GL, Patel C, Kher JA, Bhame SD. Contemporary advances in metal oxide doped polypyrrole composites: a comprehensive review. Int J Nanosci Nanotechnol. 2024;20(2):143-159. https://doi.org/10.22034/ijnn.2024.2005501.2391
34. Saravanan S, Ramalingam S, Tamilarasan G. Optical, thermal and magnetic properties of strontium ferrite nanoparticles. Int J Nanosci Nanotechnol. 2022;18(4):275-284. https://doi.org/10.22034/ijnn.2022.697998